



## OPEN

## Fatigue-Induced Damage in Zr-Based Bulk Metallic Glasses

## SUBJECT AREAS:

STRUCTURAL MATERIALS  
MECHANICAL PROPERTIES  
METALS AND ALLOYS

GLASSES

Received  
17 June 2013Accepted  
19 August 2013Published  
3 September 2013Correspondence and  
requests for materials  
should be addressed to  
P.K.L. (pliaw@utk.edu)Chih-Pin Chuang<sup>1</sup>, Tao Yuan<sup>2</sup>, Wojciech Dmowski<sup>1</sup>, Gong-Yao Wang<sup>1</sup>, Matt Freels<sup>1</sup>, Peter K. Liaw<sup>1</sup>, Ran Li<sup>3</sup> & Tao Zhang<sup>3</sup><sup>1</sup>Department of Materials Science and Engineering, the University of Tennessee, Knoxville, TN 37996, <sup>2</sup>Department of Industrial and Systems Engineering, Ohio University, Athens, OH 45701, <sup>3</sup>Department of Materials Science and Engineering, Beihang University, Beijing, China 100083.

In the present work, we investigate the effect of “fatigue” on the fatigue behavior and atomic structure of Zr-based BMGs. Fatigue experiments on the failed-by-fatigue samples indicate that the remnants generally have similar or longer fatigue life than the as-cast samples. Meanwhile, the pair-distribution-function (PDF) analysis of the as-cast and post-fatigue samples showed very small changes of local atomic structures. These observations suggest that the fatigue life of the 6-mm in-diameter Zr-based BMG is dominated by the number of pre-existing crack-initiation sites in the sample. Once the crack initiates in the specimen, the fatigue-induced damage is accumulated locally on these initiated sites, while the rest of the region deforms elastically. The results suggest that the fatigue failure of BMGs under compression-compression fatigue experiments is a defect-controlled process. The present work indicates the significance of the improved fatigue resistance with decreasing the sample size.

**B**ulk metallic glasses<sup>1–3</sup> (BMGs) will undergo mechanical fatigue even when the applied cyclic stress is far below their yielding stresses,  $\sigma_{ys}$ . The stress-strain curve indicates that the deformation of the specimen at such stress levels should be elastic, i.e., the material returns to its original state after the applied load is removed. Several researchers<sup>4–14</sup> have shown that the fatigue behavior of the Zr-based BMGs shares many similarities with crystalline materials. For example, the stress versus the number of fatigue-life-cycles (S-N) curve of a BMG resembles its crystalline counterpart, where the fatigue life is inversely proportional to the applied stress and possesses a threshold, defined as the fatigue-endurance limit (typically refers to the stress or stress range at  $10^7$  cycles). In the present article, we use the stress range,  $\Delta\sigma = |\sigma_{max} - \sigma_{min}|$ , to calculate the fatigue-endurance limit for our own results and other researchers' data, where  $\sigma_{min}$  and  $\sigma_{max}$  are applied minimum and maximum stresses, respectively. When the cyclic stress imposed on the sample is lower than the fatigue-endurance limit, the sample will not fail within  $10^7$  cycles.

The crack-propagation behavior in BMGs is similar to ductile crystalline alloys<sup>5,15</sup>. The crack-growth rate depends on the applied stress range, and striations can be observed on the fracture surface<sup>4</sup>. The fatigue-failure process of BMGs can be categorized into three stages, crack initiation, stable crack propagation, and fast fracture, as observed in crystalline alloys. The fatigue-endurance limits of the Zr-based BMGs vary significantly, ranging from  $0.05 \sim 0.5 \sigma_{ys}$ , depending on the test geometry (experiments under tension-tension, compression-compression, or bending), test materials, environments... etc. Gilbert et al.<sup>4,15</sup> first reported the fatigue behavior of the Zr-based BMG (Vitrelloy-1). They conducted four-point-bending tests on beam specimens and found that the fatigue-endurance limit was  $\sim 8\%$  of the ultimate tensile strength ( $\sigma_{UTS}$ ). Menzel et al.<sup>13</sup> later reported similar results using the same material. These early studies seem to suggest that fatigue-endurance limits of BMGs are low, compared to crystalline alloys, but other studies show that fatigue-endurance limits of BMGs can be comparable to crystalline alloys. For example, Yokoyama et al.<sup>16</sup> conducted rotating-beam fatigue tests to examine the Wohler curve of the Zr-based BMGs. The fatigue-endurance limit of the specimen in their experiments was  $\sim 57\%$  of the ultimate tensile strength. Nakai et al.<sup>17</sup> studied the fatigue-crack initiation and small crack-propagation behavior of Zr-based BMGs under tensile stresses. They reported a fatigue-endurance limit of  $52\%$  of the ultimate tensile stress. Subsequent compression-compression fatigue studies of the same material showed a slightly-lower fatigue-endurance limit of  $\sim 44\%$  of the ultimate tensile stress<sup>18</sup>. These studies show that the fatigue-endurance limits of Zr-based BMGs could vary from  $8\% \sim 57\%$  of tensile stresses. To explore the reasons behind the large variation in fatigue-endurance limits of BMGs, Launey et al.<sup>19</sup> examined the bending-fatigue behavior of Zr-based BMGs from two different manufacturers. They found that fatigue-endurance limits are



strongly affected by the free volume in the material. The differences in fatigue-endurance limits can be as large as 22% of  $\sigma_{UTS}$  (40%  $\sigma_{UTS}$  for the BMG system with less free volumes and 18%  $\sigma_{UTS}$  for the system with more free-volumes<sup>19</sup>). Wang et al.<sup>5,6,12</sup> and Peter et al.<sup>10,11</sup> performed tension-tension fatigue tests on notched Zr-based BMG samples. These tests showed that the fatigue-endurance limit is 30 ~ 50% of the ultimate tensile strength<sup>20</sup>. Wang et al.<sup>21,22</sup> suggested that several factors could affect fatigue-endurance limits, such as composition, mean stress, quality of the specimen, specimen geometry, testing environment, cyclic frequency, surface condition, etc.

Despite that fatigue behavior of Zr-based BMGs shares many similarities with crystalline alloys<sup>4-13</sup>, the mechanisms responsible for the fatigue-induced damage in BMGs are not clear. In the present work, we investigate the effect of the past “fatigue” on the fatigue behavior and atomic structure of Zr-based BMGs, aiming to provide better mechanistic understanding of fatigue characteristics of BMGs. The complete compression-compression fatigue study was conducted on the as-cast, and pre-fatigued, 6-mm in-diameter, Zr-based BMGs. The results for the as-cast samples showed a fatigue-endurance limit of 27%  $\sigma_{UTS}$ , while the pre-fatigue-to-failure samples exhibited similar or more cycles-to-failure. The local atomic-structure characterization using the high-energy synchrotron X-ray pair-distribution-function (PDF) analysis showed very small changes of local atomic structures. Statistical analyses of the fatigue data imply a possible size effect<sup>23-26</sup>, which affects the fatigue life, i.e., the smaller the sample size, the higher the chance the sample will last longer under cyclic-compression loading. These results suggest that the fatigue life of the 6-mm in-diameter Zr-based BMGs is dominated by the number of pre-existing crack-initiation sites in the sample, and once the crack initiates, the fatigue-induced damage accumulates locally on these initiated sites, while the rest of the region deforms elastically.

## Results

The BMGs used in the current study are cylindrical rods with the composition of (Zr<sub>55</sub>Cu<sub>30</sub>Ni<sub>5</sub>Al<sub>10</sub>)<sub>98</sub>Er<sub>2</sub> in atomic percent (at.%), a diameter (D) of 6 mm, and a length (L) of 25 mm. Samples were fatigued under a compression-compression mode. The details of the experiment can be found in the “Methods” section. The test was ended when the sample was fractured. Then the sample was collected for visual inspections. The undamaged part after cutting out the fracture surface was preserved for the 2<sup>nd</sup>-round fatigue experiment using the same testing conditions. The sample for the 2<sup>nd</sup>-run fatigue has smaller L/D ratios since the length is shorter. The same procedure was repeated until the L/D ratio of the leftover was less than 0.8. The fatigue tests of each run were recorded for analyses.

The schematic diagram of the above experimental plan is shown in Figure 1. Note that cutting of the damaged parts was purely determined by visual inspection. It is possible that there are hidden cracks inside the sample. These pre-existing cracks will certainly have a strong impact on the fatigue life during the 2<sup>nd</sup> test. Two out of six samples failed within few cycles of the second tests. These samples were excluded from our analysis, since they most likely had pre-existing cracks from the first test.

The structures of the as-cast and fatigued specimens were characterized by a high-energy X-ray diffraction (HEXRD) technique [Sup-1(a)]. The cylindrical samples with a diameter of 6 mm were cut into a 1-mm-thick plate with the plane normal to the loading direction, as shown in Sup-1(b), and were examined using 100 keV (with a wavelength,  $\lambda_{avg} = 0.12398 \text{ \AA}$ ) radiation in a transmission geometry. The intensity of the scattered X-rays was collected by a MAR345 image plate. The experimental geometry is illustrated in Sup-1. The data were processed and converted into tables of the scattering intensity versus scattering angle,  $\theta$ , employing the FIT2D software<sup>27</sup>.

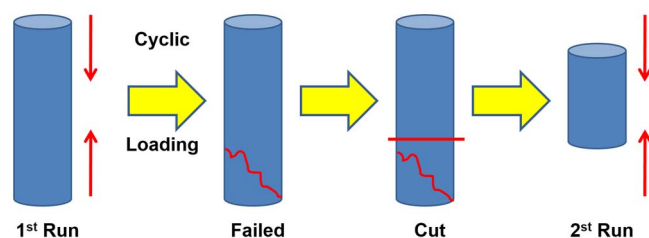


**Figure 1 | A schematic diagram of the experimental design.** The as-cast sample undergoes compression-compression fatigue until it fails. Then, the damaged part is cut off, and the leftover is used for the next fatigue test as long as the rest part has an L/D ratio greater than 0.8.

To further examine the effect of cyclic loading on the short-range atomic structure, the PDF analysis was performed. The measured scattering intensity,  $I(Q)$  ( $Q = 4\pi \sin \theta / \lambda$ , where  $\theta$  is the diffraction angle, and  $\lambda$  is the wavelength), was integrated over the azimuthal direction, and corrected for the polarization effect, fluorescence background, absorption, inelastic scattering, and the scattering from the air and container using the methods described in Ref. 28<sup>28</sup> to obtain the structure function,  $S(Q)$ . The corresponding PDF,  $G(r)$ ,

$$G(r) = \frac{2}{\pi} \int_0^\infty [S(Q) - 1] \sin(Qr) Q dQ \quad (1)$$

was obtained by the Fourier transformation of  $S(Q)$ , where  $S(Q)$  is the structure factor, and  $r$  is the atomic-pair distance.

The failed specimen was sliced vertically along the loading axis, as shown in Sup-1(c), and the structure characterization was performed along the loading direction. This geometry allows us to characterize the anisotropy term of the specimen under cyclic compression. In addition, the microstructures of the regions near and away from the fracture plane can be compared.

Figure 2(a) shows the S-N curve of the as-cast (Zr<sub>55</sub>Cu<sub>30</sub>Ni<sub>5</sub>Al<sub>10</sub>)<sub>98</sub>Er<sub>2</sub> alloy, and the results of the series of fatigue tests from the current study. The open circle is the fatigue life of the studied material with a fixed L/D ratio of 1.67, and a testing frequency of 10 Hz at various stress ranges (typical fatigue tests). The colored symbols are the data from this study (a larger L/D ratio). The red color denotes the first-cycle tests (as-cast samples), and the blue color represents the proceeding tests using the leftover from the first fatigue test. The number of cycles-to-failure of each test was counted individually; the fatigue life of 2<sup>nd</sup>-run or 3<sup>rd</sup>-run tests excluded the prior fatigue history. The first-cycle tests of the specimens show comparable fatigue life with one sample on the left side of the S-N curve and two samples on the right side of the S-N curve [red symbols in Figures 2(a) and (b) and Table I]. For the second-cycle tests (blue symbols), it is seen that the fatigue life is comparable or longer when compared with the 1<sup>st</sup>-cycle test (the as-cast condition). To clearly show these results, we plot the fatigue data, separately, in Figure 2(b), and the detailed data are summarized in Table I.

Many factors, such as the frequency of the test and the geometry of the specimen, will affect the fatigue behavior of BMGs<sup>21</sup>. Since the same sample is used for several runs of the tests, the sample will inevitably become progressively smaller. The changes of L/D ratios might affect the fatigue life of a specimen. We plot the fatigue life of each test as a function of L/D ratio in Figure 2(c). The results do not show strong correlation between the L/D ratio and the fatigue life within the L/D range from approximately 0.8 to 4. Therefore, the dominant factor that affects the fatigue life of a specimen in this experiment could be related to cyclic loading.

To further identify the failure mechanism of the fatigue tests, we examine the fracture surface by scanning-electron-microscopy (SEM). The images are shown in the supplement material. Sup-2 presents the surface morphology of the fracture specimen. A

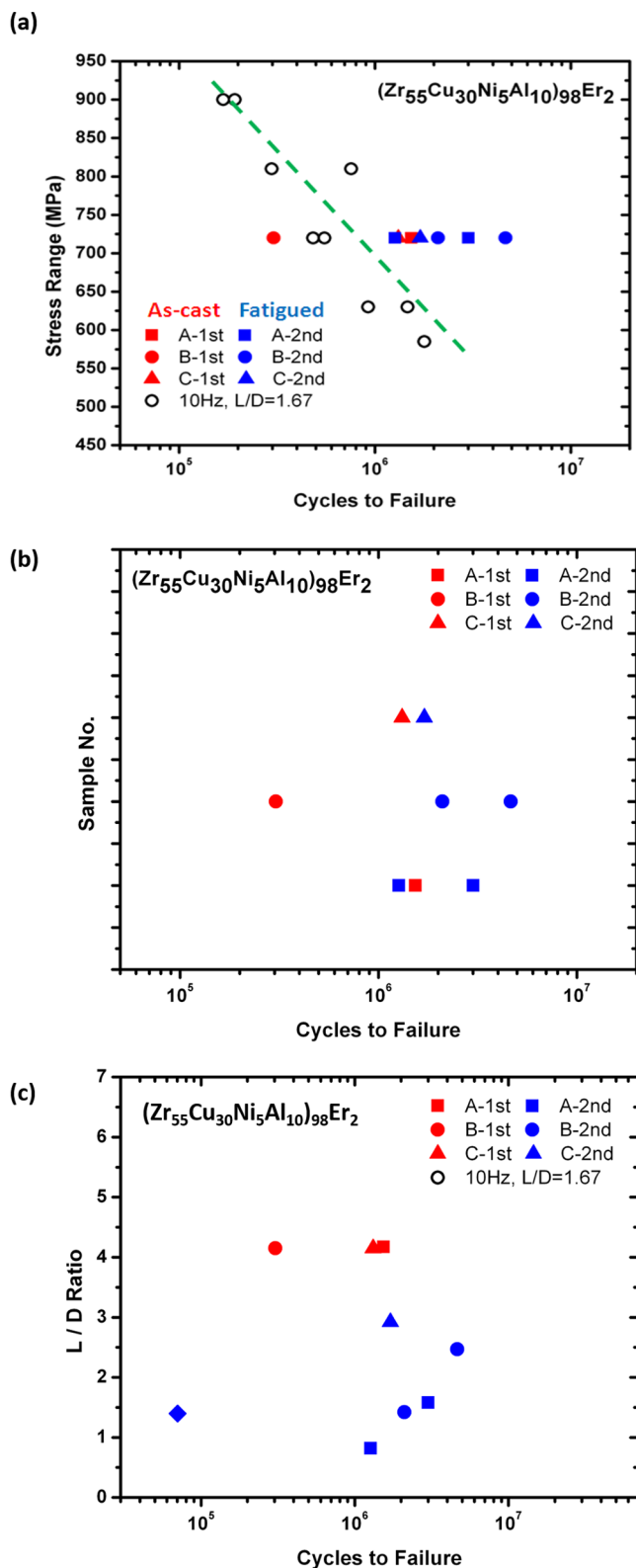


**Figure 2** | (a) The stress-range versus number of cycles to failure (S-N curve) data of  $(\text{Zr}_{55}\text{Cu}_{30}\text{Ni}_5\text{Al}_{10})_{98}\text{Er}_2$  BMGs. The open circle is the fatigue life of the same material with a fixed L/D ratio ( $L/D = 1.67$ ), and a frequency of 10 Hz at various stress ranges. The colored symbols are the data from this study. (b) The fatigue life of samples, A, B, and C. The 1<sup>st</sup>-run (in the as-cast condition) data is shown in red, and the 2<sup>nd</sup> run data is presented in blue. The number of cycles-to-failure of the 2<sup>nd</sup>-run test starts from zero, and does not include the cycles made in the 1<sup>st</sup>-run test. The fatigue life of the “pre-fatigued” sample (leftover) is equal or longer,

compared to the as-cast sample. The results suggest that the fatigue damage in the specimen is mainly localized, and cyclic loading has no globalized effect on the sample. When the fractured part is removed, the rest of the material acts just like an as-cast material. (c) The number of cycles to failure as a function of the L/D ratio of the specimen. The results showed no correlation between the L/D ratio and the fatigue life.

characteristic vein-like pattern, as shown in Sup-2(a) and the left side of Sup-2(c), is observed on the fracture surfaces. This pattern is commonly found on the fracture surface of BMGs under tension or compression tests<sup>12,15</sup>. These features are believed to be formed during the final stage (fast fracture) of the fatigue fracture, when the stress on the remaining load-carrying cross-section of the sample reaches the load limit of the material, and the spread of fracture becomes catastrophic. Then the material on the shearing plane becomes melted due to the heat generated during the fracture process at the fast fracture stage. Striations, as shown in Sup-2(b) and (c), could be found only on a small portion of the fracture surface. Sup-2(b) is the enlarged view of the rectangle in Sup-2(c). A molten droplet covers a part of the striation. The striation spacing is  $\sim 190$  nm. It is unusual to observe striations during the fatigue failure of BMGs under cyclic compression-compression loadings. These trends are commonly seen on the fatigue tests under bending conditions. The striations have not been reported before for Zr-based BMGs under cyclic compression-compression fatigue (although previous studies usually used samples with smaller diameters ( $< 3$  mm)). We could not locate the crack-initiation sites on the fracture surface, since they were destroyed by surface melting due to severe shearing at the final stage of the fatigue failure.

The as-cast and two fatigued samples were examined by synchrotron high-energy X-ray diffraction. The spectra of three samples show identical features without the sign of the presence of crystalline phases (Sup-3). The present result indicates that the specimens before and after fatigue tests are in an amorphous state, without any major structure changes (phase transformations). We obtained the PDF shown in Figure 3(a) by the Fourier transformation of the structure function,  $S(Q)$ , to study the local atomic structure of the amorphous samples. We compare the  $G(r)$  of an as-cast sample to that of a fatigued sample. The differences between as-cast and fatigued samples are very small [We only show  $G(r)$  of sample B in Figure 3(a) for comparison]. The results suggest that there is no significant changes on the atomic structure of the BMG in the medium-range ( $> 10$  Å) region, but only small differences in the short-range ( $< 5$  Å) region. Since the changes in the short-range region are rather small (less than  $\sim 0.6\%$ ), we used a standard statistical tool, the two-way analysis of variance, to test whether this difference is significant. We tested the difference in  $G(r)$  between as-cast and fatigued specimens,  $\Delta G(r) = G(r)^{\text{fatigued}} - G(r)^{\text{as-cast}}$ , [in Figure 3(a)] and the first derivative of  $\Delta G(r)$  of the same sample measured at different places [the same sample measured at 1-ID and 11-ID beamlines of the Advanced Photon Source (APS), Argonne National Laboratory, using the same experimental setup]. The statistical analysis showed that the differences are not significant.

**Table 1** | The table of fatigue data in Figure 2

	1st		2nd	
	cycle to failure	L/D	cycle to failure	L/D
A	1,535,442	4.17	1,269,216	0.82
B	304,354	4.15	3,003,711	1.58
			2,100,754	1.83
C	1,315,717	4.15	4,639,253	1.4
			1,703,792	2.92

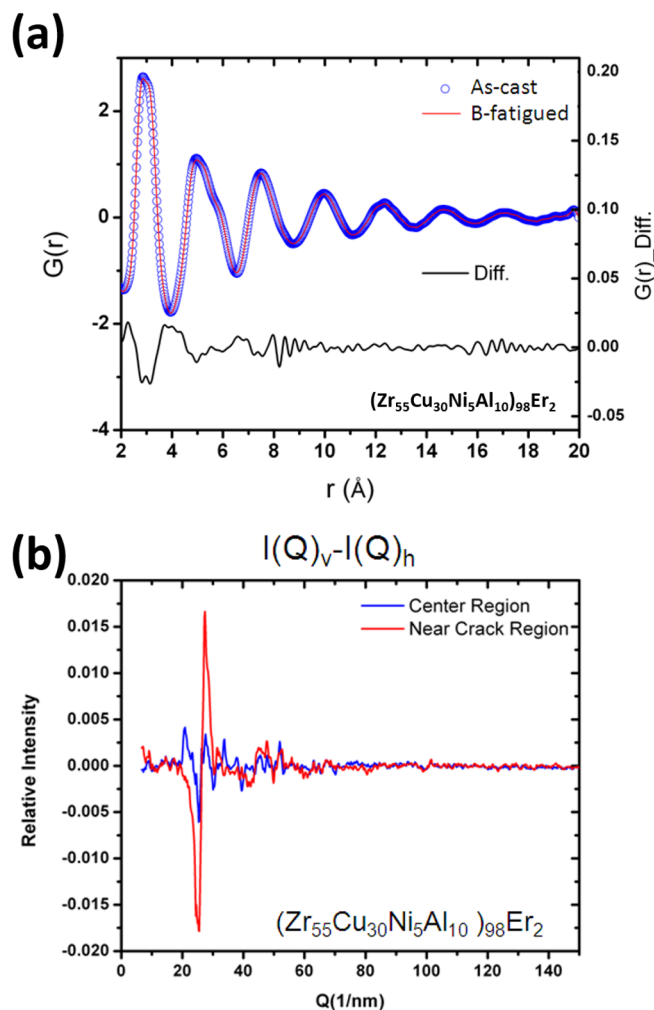


**Figure 3** | (a) Reduced pair-distribution functions of the as-cast and fatigued samples. No significant changes between the as-cast and fatigued samples were found, but we do observe small differences in the short-range-order part (within 8 Å). (b) A very small but notable diffraction anisotropy, found in the fracture-surface region. It might result from severe plastic deformation inside the shearing plane at the final stage of the failure (fast cracking).

We compared  $I(Q)$  between the center region and the near-fracture-surface section of the sample, as illustrated in Sup-1(c). No significant differences can be observed in both  $I(Q)$  and  $G(r)$ . With the measurement geometry used in Sup-1(c), we could compare the diffraction anisotropy of the samples after fatigue tests. To reveal the diffraction anisotropy, we subtract the  $I(Q)$  in the horizontal direction (the transverse direction) from the  $I(Q)$  in the vertical direction (the loading direction). The result in Figure 3(b) showed that the diffraction anisotropy can only be observed near the fracture-surface region, and the magnitude is small ( $< 0.6\%$ ); while in the bulk region, the structure of the sample is still isotropic. The anisotropic behavior is likely caused by severe shearing in the fast-fracture stage, the last stage of the fatigue failure of the BMG, not the cyclic loading itself<sup>29</sup>.

The schematic diagram of the fatigue experiment is shown in Figure 1. The experiment is a series of constant-load compression-fatigue tests. For the first run, denoted as the 1<sup>st</sup> run, an as-cast BMG specimen is used. The repeated loading/unloading fatigue process continues until the specimen fails. Then, the broken/damaged region is removed, as illustrated in the figure, and the leftover is used for the 2<sup>nd</sup>-run test. The experimental condition

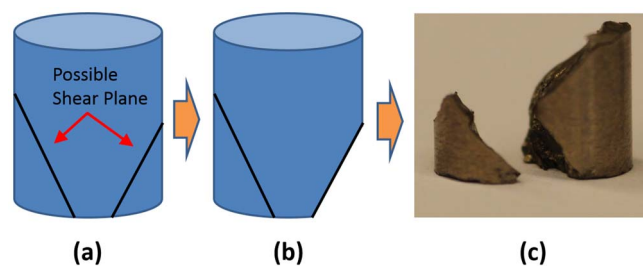


**Figure 4** | Possible failure mode of the large-diameter BMG under cyclic-compression stresses. (a) Some of the possible shear planes do not cut through the whole specimen, but start from the end of the specimen. (b) When a small piece of the sample was separated from the major part, the stress on the load-carrying cross-section of the sample is still less than the strength of the material. The situation became as if we were running a fatigue test using an irregularly-shaped specimen with higher stress levels. (c) A failed 6-mm-in-diameter specimen in the present study.

of the 2<sup>nd</sup>-run test is identical to the 1<sup>st</sup>-run test, except that the sample is shorter, since the fractured region was removed. The series of tests was continued until the L/D ratio of the leftover was less than 0.8. Jiang et al.<sup>30</sup> studied the effect of sample geometry on the deformation behavior of Zr-based BMGs under compression experiments. They confirmed that as long as the L/D ratio is larger than 0.75, it will not affect the fracture mode and mechanism of BMGs under compression. Therefore, we only used samples with L/D larger than 0.8 for continuing the fatigue experiments.

Comparing the fatigue life of each run helps clarify mechanisms of fatigue damage of BMGs. If the fatigue life of the 2<sup>nd</sup>-run test is longer than the 1<sup>st</sup>-run test, then the fatigue test produces only localized damage to the specimen. Once the crack is initiated, the damage is mainly accumulated around the existing crack, while the remaining part of the sample still undergoes elastic deformation. After the damaged region is removed, the rest of the sample is just like the as-cast sample but with fewer defects, since the weakest point of defects in the specimen has been screened out by the 1<sup>st</sup>-run fatigue test. Hence, the next fatigue test will show longer fatigue life than the first one. On the other hand, if the 1<sup>st</sup>-run test had the longer fatigue life than the 2<sup>nd</sup>-run test, cyclic loading produces globalized damage to the specimen. The crack will initiate more easily on the fatigued specimen. Therefore, the fatigue life will be shorter. In the present study, we found that the 2<sup>nd</sup>-run test has similar or longer fatigue life than the 1<sup>st</sup>-run test. Thus, the fatigue life of a large diameter specimen under a compressive stress could be controlled by the number of pre-existing crack-initiation sites (defects) in the specimen.

Similar to the samples with smaller diameters, fracture of larger-diameter samples under cyclic compression mostly occurred in a pure shear mode. The major fracture plane formed an angle of  $\sim 42^\circ$  with respect to the loading axis<sup>31,32</sup>. However, unlike the smaller samples in which the major shear plane passes through the whole specimen and separates the specimen into two pieces with a relatively flat shear plane, these larger samples usually broke into multiple pieces, with a convex-shaped major shear plane. The fracture morphology of the fatigued cylindrical specimen with different diameters are showed in Sup-4. This phenomenon could be explained as follow. During the fatigue test, there are many possible shear planes for cracks to form. Some of the possible shear planes do not cut through the whole specimen, but start from the end of the specimen, as illustrated in Figure 4(a). When a shear plane formed from the side surface to the end of the specimen, a small piece of the sample will be removed, as shown in Figure 4(b). Because the sample is large, the stress on the load-carrying cross-section of the sample is still less than the strength of the material. As a result, the fatigue test is carried out on an irregularly-shaped specimen with higher-stress levels. The odd shape of the sample creates a fairly complex stress state within the





specimen, and further diversifies the final failure mode of the sample as shown in Figure 4(c). This peculiar mode creates difficulty to identify the failure mechanism of large BMGs specimens under compression-compression fatigue tests, since crack-initiation sites and crack-propagation regions [as shown in Sup-2(c)] are destroyed by severe shearing during the final stage of the failure.

In Figure 2(c), we have shown that the fatigue life does not strongly correlate with the L/D ratio of the specimen. However, the sample volume also changed between the fatigue tests and become progressively smaller. Then the size effect on the fatigue behavior of BMGs should be examined. In the following section, we use statistical analyses to examine the effect of sample size on the fatigue life.

A statistical model is developed to predict the fatigue life of the BMG based on the defect volume. We hypothesize that the fatigue life can be characterized by the Weibull theory<sup>33</sup>. The Weibull theory assumes that the fatigue failure is determined by the presence of a critical defect, and such defects occur randomly within a material<sup>33</sup>. As a consequence, specimens with larger volumes will have greater probability of finding a critical defect, and, therefore, have statistically shorter fatigue lives when compared with specimens with smaller volumes<sup>34,35</sup>.

The two-parameter Weibull fatigue-life distribution has the following cumulative distribution function,

$$F(N|\alpha, \beta) = 1 - \exp \left[ -V \left( \frac{N}{\alpha} \right)^\beta \right] \quad (2)$$

where  $N$  denotes the number of cycles to failure, and  $V$  is the volume of the test specimen. This model has two parameters,  $\alpha$  and  $\beta$ .  $\alpha$  is the characteristic fatigue life of a unit volume, and  $\beta$  is the Weibull fatigue modulus<sup>33,35</sup>. The probability density function of the Weibull fatigue-life distribution is

$$f(N|\alpha, \beta) = V \frac{\beta}{\alpha} \left( \frac{N}{\alpha} \right)^{\beta-1} \exp \left[ -V \left( \frac{N}{\alpha} \right)^\beta \right] \quad (3)$$

Given the number of cycles to failure and the volumes of  $n$  test specimens, denoted by  $N_i$  and  $V_i$ , respectively, for  $i = 1, \dots, n$ , the unknown parameters,  $\alpha$  and  $\beta$ , can be estimated by the maximum likelihood method<sup>36</sup>. The maximum likelihood estimates of  $\alpha$  and  $\beta$  maximize the likelihood function given by

$$L(\alpha, \beta|N_1, \dots, N_n, V_1, \dots, V_n) = \prod_{i=1}^n V_i \frac{\beta}{\alpha} \left( \frac{N_i}{\alpha} \right)^{\beta-1} \exp \left[ -V_i \left( \frac{N_i}{\alpha} \right)^\beta \right] \quad (4)$$

The Weibull theory implies a volume-scaling relation between the fatigue life and the specimen volume. Assuming equal failure probabilities, the volume effect on the fatigue-life ratio for two specimens of volumes,  $V_A$  and  $V_B$ , is

$$\frac{N_A}{N_B} = \left( \frac{V_B}{V_A} \right)^{1/\beta} \quad (5)$$

where  $N_A$  and  $N_B$  are the respective fatigue lives. This volume scaling relation suggests a possible way to assess the goodness-of-fit of the Weibull fatigue-life model, given a small amount of failure data, by scaling all the observed fatigue lives to a reference volume. If the Weibull model is an appropriate method to describe the variability in the data and the volume effect, the scaled fatigue lives at the reference volume should follow a Weibull distribution.

Table II lists the volumes and the fatigue lives of ten specimens tested at a stress range of 720 MPa. The MATLAB Optimization Toolbox is used to maximize the likelihood function, Equation (4). The maximum likelihood estimates of the two-model parameters are  $\beta = 1.453$  and  $\alpha = 115.323$  million cycles.

**Table II | Volumes and fatigue lives of ten experimental specimens**

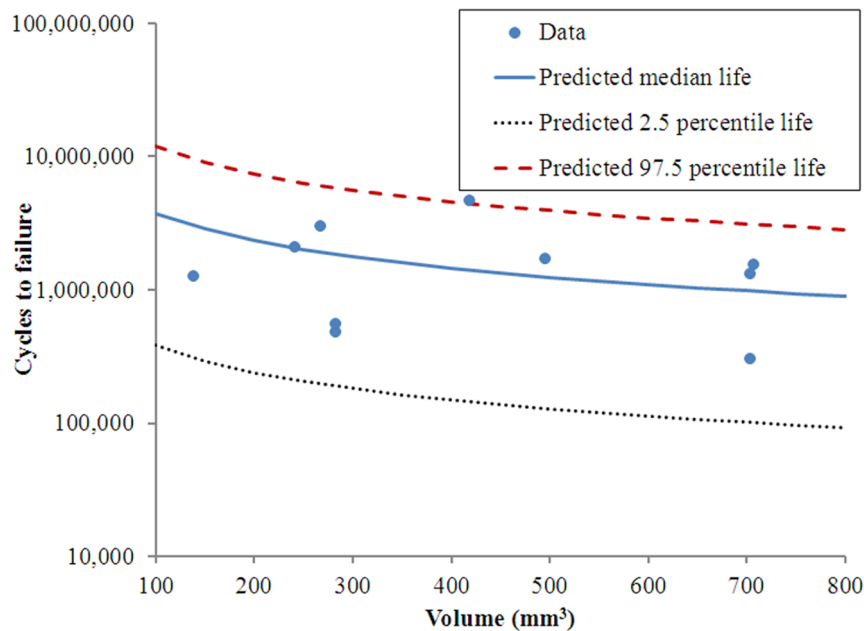
Sample, $i$	Volume, $V_i$ (mm <sup>3</sup> )	Cycles to failure, $N_i$ (million cycles)
1	282.7433	0.484017
2	282.7433	0.552864
3	707.4238	1.535442
4	704.0309	0.304354
5	704.0309	1.315717
6	139.1097	1.26922
7	268.0407	3.00371
8	495.3663	1.70379
9	240.8973	2.10075
10	419.0256	4.63925

Figure 5 shows the predicted median, 2.5 percentile, and 97.5 percentile lives. The 2.5 and 97.5 percentiles form a 95% predictive interval. This 95% predictive interval captures almost all the observations. Only one observation falls outside the predictive interval. To assess the goodness-of-fit of the Weibull fatigue-life model<sup>33</sup>, all the observed numbers of cycles-to-failure are scaled to a reference volume of 700 mm<sup>3</sup> according to Equation (5). We then perform a statistical hypothesis test to determine whether the Weibull theory can be used to explain the volume dependence in the S-N data. Two competing hypotheses denoted by  $H_0$  and  $H_1$  are formulated as:  $H_0$  - the scaled fatigue lives follow the Weibull distribution, and  $H_1$  - the scaled fatigue lives do not follow the Weibull distribution. The Anderson-Darling goodness-of-fit test is applied to decide which hypothesis is true; and the test yields a P-value of 0.202, which supports  $H_0$ . Thus, this analytical result indicates that Weibull theory may be used to explain the variability in the data as well as the volume dependence of the fatigue life (i.e., a smaller-volume sample tends to exhibit a longer fatigue life, Figure 5).

We used the Weibull theory to describe the fatigue behavior of this material from the statistical point-of-view. According to the analytical results, the Weibull fatigue-life prediction method seems to be an appropriate model to describe the variability in the observed fatigue data and the volume effect. The fatigue behavior of this material, therefore, may be explained by the Weibull theory. Although statistical analyses imply the possible size-dependent fatigue behavior (i.e., a smaller-volume sample tends to exhibit longer fatigue life, Figure 5), more experimental and analytical work, however, needs to be conducted to warrant the conclusions.

## Discussion

Recent studies of fatigue behavior of metallic-glass (MG) nanowires by computer molecular-dynamic simulations<sup>37</sup> showed that MGs will not fatigue. Shi et al.<sup>37</sup> simulated the fatigue behavior of MG nanowires under strain-controlled compression-compression tests and found that “irreversible deformation occurs during all fatigue simulations”. However, the MG nanowire does not suffer from structural damage, and no softening occurs during cyclic loading<sup>37</sup>. Jang, Gross, and Greer<sup>14,23</sup> reported a significant strength increase and highly-localized-to-homogeneous deformation mode change, when the size of the MG nanowire decreases to a nano-meter scale. The strength of the MG pillar starts increasing with decreasing the diameter at a micro-meter scale, and reaches its maximum value of 2.6 GPa at a diameter of 800 nm, compared to the yield strength of 1.7 GPa in the bulk (millimeter) scale. Below a diameter of 800 nm, the yield strength of the MG nano-pillar remains unchanged. However, there is a change of the deformation mechanism from a highly-localized shear-deformation mode to homogeneous viscous flow at a diameter of 100 nm. Jang et al.<sup>38</sup> further studied the fatigue behavior of MG micron-sized pillars and found that the fatigue-endurance limit is generally very close to the yield strength of BMGs, i.e., MGs will not fatigue at submicron scales. The experimental results are consistent with Shi et al.’s molecular-dynamic



**Figure 5** | Predicted percentile lives by the Weibull fatigue-life model.

(MD) simulations<sup>37</sup>. These studies<sup>14,23,37</sup> showed that the size of the specimen does affect the fatigue behavior of amorphous alloys under compression-compression fatigue, i.e., smaller-size samples generally exhibit longer fatigue life, as generally observed in Figure 5. However, the results from the present study, Figure 5, do not show very strong size-dependent behavior. The reason is likely due to the fact that the sizes of the specimens used in the current study are on the millimeter scale. The size effect on the compression-compression fatigue could be pronounced at a micro-meter scale or below<sup>14,23,37</sup>.

Wang, Yuan et al.<sup>20,22</sup> studied the effect of specimen size on the fatigue behavior of Zr-based BMGs under 4-point bending tests. They reported that the smaller-sized sample (2 mm × 2 mm × 25 mm) has shorter lifetime and a lower fatigue-endurance limits than the large-sized sample (3 mm × 3 mm × 25 mm). Their results are different from what we observed in the present study. The inconsistency is most likely due to the different fatigue-fracture mechanisms between bending-fatigue and compression-compression-fatigue tests. In bending fatigue, the small-sized BMG samples show the flexural and fracture failure, while the large-sized BMG samples only exhibit the fracture failure. Due to the improved bend ductility of the small-sized BMG sample, more multiple shear bands can form easily than the large-sized sample under cyclic loading. The cracks initiated from these shear bands. Thus, in the small-sized BMG sample during the bending test, multiple shear bands act as weak spots initiating cracks, which shortens the fatigue life, relative to the large-sized sample<sup>20,22</sup>. On the other hand, in compression-compression-fatigue tests, crack initiation is associated with critical flaws (the weakest point) in the sample. The probability of having these flaws scales with the size (volume) of the sample. Therefore, smaller samples might have longer fatigue life under compression-compression fatigue.

From several research papers<sup>5,10,11,39–42</sup>, one can categorize the fatigue failure of BMGs into three stages. The first is the crack-initiation stage, where a crack is initiated at the weakest point of the material, followed by the crack-propagation stage, where the crack advances slowly under the repeated loading and unloading fatigue process; and finally, the fast propagating stage, which causes the final failure of the material. The crack-initiation stage is the key to determine the fatigue life of such materials with very little or no plasticity. The fatigue-crack-initiation sites in BMGs could be further divided

into two groups. Type-I is defects, such as free volumes and/or shear bands, which is associated with the nature of amorphous alloys, and Type-II is related to the defects, such as inclusions, micro-voids, and nano-crystalline particles formed during the fabrication process, which, theoretically, can be eliminated by better fabrication techniques and/or procedures.

From this study, the fatigue-failure mechanism of the large (6-mm in-diameter) Zr-based BMGs under cyclic compression-compression stresses is suggested, and illustrated in Figure 6. The crack initiates at the weakest points (extrinsic defect sites as defined above) in the sample. The crack propagates slowly at the beginning and leaves the striation on the crack surface. The crack continues to grow until the sample cannot sustain the stress, and then the fast-shearing process starts, which causes the catastrophic failure. During the crack-propagation process, the fatigue damage is localized. When one crack

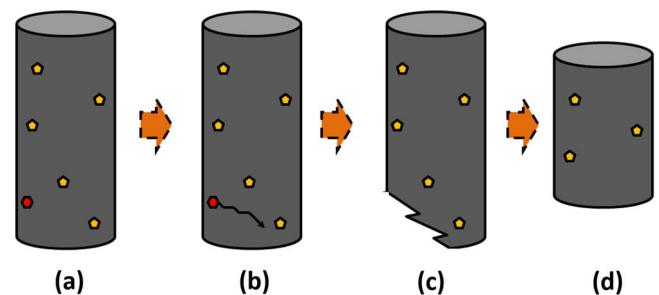


**Figure 6** | Proposed fatigue-failure mechanisms of the large (6-mm in-diameter) (Zr<sub>55</sub>Cu<sub>30</sub>Ni<sub>5</sub>Al<sub>10</sub>)<sub>98</sub>Er<sub>2</sub> BMGs. (a) The as-cast sample contains weak points (defect sites, such as microvoids or nanocrystalline particles formed during the fabrication process). (b) The crack initiates at the weakest point in the sample. The crack propagates slowly at the beginning, and leaves the striation on the crack surface. (c) The crack continues to grow until the sample cannot sustain the stress and then starts fast shearing of the sample (fast fracture). The fatigue damage is found to be localized. When one crack starts to grow, the rest of the sample still undergoes elastic deformation. The microstructure away from the crack region generally remains unchanged. (d) Therefore, after cutting off the damaged part, the remaining material performs like an as-cast material with less defects.



starts to grow, the rest of the sample still undergoes elastic deformation; the microstructure away from the crack region generally remains unchanged. Therefore, after cutting off the damaged part, the remaining part performs like an as-cast material. The above mechanism implies that the fatigue-endurance limit of BMGs under cyclic compression-compression stresses can be greatly improved by reducing the number of Type-II defects (crack-initiation sites) in the material.

In conclusion, we investigated the effect of “pre-fatigue” on the fatigue behavior and atomic structure of Zr-based BMGs, aiming to provide better mechanistic understanding of the fatigue process in BMGs. The complete compression-compression fatigue study was conducted on the as-cast, 6-mm in-diameter, Zr-based BMGs. The fatigue-endurance limit and the fatigue ratio of this material were 500 MPa and 0.27, respectively. Fatigue experiments on the pre-fatigue-to-failure samples indicated that these leftovers generally had similar or longer numbers of cycles-to-failure than the as-cast samples. The PDF analysis of the as-cast and post-fatigue samples, using the high-energy synchrotron X-ray scattering method, showed very small changes of local atomic structures. The results suggest that the fatigue life of the 6-mm in-diameter Zr-based BMG is dominated by the number of pre-existing crack-initiation sites in the sample. Once the crack initiates, the fatigue-induced damages are accumulated locally on these initiated sites, while the rest of the region deforms elastically. The statistical model predicts that the fatigue life of BMGs under compression-compression fatigue tests may be longer when the size of the sample decreases. The results from the present study imply that the fatigue failure of BMGs under compression-compression fatigue tests is a defect-controlled process. The current research indicates the importance of the improved fatigue resistance with reducing the sample size. This phenomenon has far-reaching implications of BMGs in small volumes under cyclic compression-compression loading.

## Methods

The BMGs used in the current study were prepared by arc-melting high-purity elements, Zr (99.99 mass%), Cu (99.99 mass%), Ni (99.99 mass%), Al (99.99 mass%), and Er (99.99 mass%), under argon atmosphere. The alloy composition is  $(\text{Zr}_{55}\text{Cu}_{30}\text{Ni}_{15}\text{Al}_{10})_{98}\text{Er}_2$  in atomic percent (at.%). To ensure the homogeneity of the sample, the ingots were re-melted several times before tilt-casting into cylindrical rods with a diameter of 6 mm, and a length of 60 mm. Since the sample is relatively large (6 mm in diameter and 60 mm in length), different cooling rates might exist between the top (closer to the crucible) and the lower ends of the specimen. Only the lower halves (away from the crucible) of the specimens, which have higher cooling rates, were used in this study to minimize the possible cooling-rate effect, because BMGs are sensitive to the thermal history during the fabrication process. Higher cooling rates usually yield better quality.

The as-cast sample was cut into a 25-mm long cylindrical rod by electric-discharge machining (EDM). The purpose of using EDM is to minimize the mechanical damage of the sample during the cutting process, and to make sure that both ends are parallel to each other. It is important to maintain the parallelism of the sample in compression-compression fatigue experiments, since unbalanced loading will greatly affect the fatigue life of BMGs. For each specimen, two thin slices about ~1-mm thick were cut by EDM from the top and the bottom ends to examine the quality of the specimen. The structure of both slices was characterized by high-energy synchrotron X-ray diffraction (HEXRD) and differential scanning calorimetry (DSC). Both tests indicated that the as-cast samples were in an amorphous state. No sharp diffraction peak from crystalline particles was observed, and the as-cast sample showed the distinct glass-transition ( $T_g$ ) and crystallization ( $T_x$ ) event upon heating, with the temperatures of 408°C and 483°C, respectively.

The as-cast, 6 mm in-diameter and 25 mm in-length rods are used for the fatigue tests. Samples were fatigued under a load-control mode at a fixed stress range of 720 MPa, a load ratio  $R$ , the minimum stress ( $\sigma_{\min}$ ) divided by the maximum stress ( $\sigma_{\max}$ ), equal to 10 (i.e.,  $R = 10$ ,  $\sigma_{\max} = -80$  MPa, and  $\sigma_{\min} = -800$  MPa), and a frequency of 2 Hz using a sinusoidal waveform. The stress level was selected, based on the regular fatigue test of the same material with the same diameter under similar testing conditions (10 Hz, a fixed  $L/D$  ratio of 1.67, where  $L$  is the length of the specimen, and  $D$  is the diameter of the specimen). At this stress range, the fatigue life is around  $\sim 8 \times 10^5$  cycles.

1. Byrne, C. J. & Eldrup, M. Materials science - Bulk metallic glasses. *Science* **321**, 502–503 (2008).

2. Wang, W. H. Bulk Metallic Glasses with Functional Physical Properties. *Advanced Materials* **21**, 4524–4544 (2009).
3. Lewandowski, J. J. & Greer, A. L. Temperature rise at shear bands in metallic glasses. *Nature Materials* **5**, 15–18 (2006).
4. Gilbert, C. J., Lippmann, J. M. & Ritchie, R. O. Fatigue of a Zr-Ti-Cu-Ni-Be bulk amorphous metal: Stress/life and crack-growth behavior. *Scr. Mater.* **38**, 537–542 (1998).
5. Wang, G. Y. *et al.* Fatigue behavior and fracture morphology of  $\text{Zr}_{50}\text{Al}_{10}\text{Cu}_{40}$  and  $\text{Zr}_{50}\text{Al}_{10}\text{Cu}_{30}\text{Ni}_{10}$  bulk-metallic glasses. *Intermetallics* **12**, 1219–1227 (2004).
6. Wang, G. Y. *et al.* Comparison of fatigue behavior of a bulk metallic glass and its composite. *Intermetallics* **14**, 1091–1097 (2006).
7. Harlow, D. G., Liaw, P. K., Peter, W. H., Wang, G. Y. & Buchanan, R. A. An approach to modeling the S-N behavior of bulk-metallic glasses. *Acta Mater.* **56**, 3306–3311 (2008).
8. Tatschl, A., Gilbert, C. J., Schroeder, V., Pippan, R. & Ritchie, R. O. Stereophotogrammetric investigation of overload and cyclic fatigue fracture surface morphologies in a Zr-Ti-Ni-Cu-Be bulk metallic glass. *J. Mater. Res.* **15**, 898–903 (2000).
9. Wu, Y. A., Xiao, Y. H., Chen, G. L., Liu, C. T. & Lu, Z. P. Bulk metallic glass composites with transformation-mediated work-hardening and ductility. *Advanced Materials* **22**, 2770–2773 (2010).
10. Peter, W. H., Buchanan, R. A., Liu, C. T. & Liaw, P. K. The fatigue behavior of a zirconium-based bulk metallic glass in vacuum and air. *Journal of Non-Crystalline Solids* **317**, 187–192 (2003).
11. Peter, W. H. *et al.* Fatigue behavior of  $\text{Zr}_{52.5}\text{Al}_{10}\text{Ti}_5\text{Cu}_{17.9}\text{Ni}_{14.6}$  bulk metallic glass. *Intermetallics* **10**, 1125–1129 (2002).
12. Wang, G. Y. *et al.* Fatigue behavior of Zr-Ti-Ni-Cu-Be bulk-metallic glasses. *Intermetallics* **13**, 429–435 (2005).
13. Menzel, B. C. & Dauskardt, R. H. Stress-life fatigue behavior of a Zr-based bulk metallic glass. *Acta Mater.* **54**, 935–943 (2006).
14. Jang, D. & Greer, J. R. Transition from a strong-yet-brittle to a stronger-and-ductile state by size reduction of metallic glasses. *Nature Materials* **9**, 215–219 (2010).
15. Gilbert, C. J., Schroeder, V. & Ritchie, R. O. Mechanisms for fracture and fatigue-crack propagation in a bulk metallic glass. *Metallurgical and Materials Transactions a-Physical Metallurgy and Materials Science* **30**, 1739–1753 (1999).
16. Yokoyama, Y. *et al.* Fatigue-strength enhancement of cast  $\text{Zr}_{50}\text{Cu}_{40}\text{Al}_{10}$  glassy alloys. *Mater. Trans.* **47**, 1286–1293 (2006).
17. Nakai, Y. & Hosomi, S. Fatigue crack initiation and small-crack propagation in Zr-based bulk metallic glass. *Mater. Trans.* **48**, 1770–1773 (2007).
18. Nakai, Y., Sakai, K. & Nakagawa, K. Fatigue of Zr-based bulk metallic glass under compression-compression stress. *Advanced Engineering Materials* **10**, 1026–1029 (2008).
19. Launey, M. E., Busch, R. & Kruzic, J. J. Influence of structural relaxation on the fatigue behavior of a  $\text{Zr}_{41.25}\text{Ti}_{13.75}\text{Ni}_{10}\text{Cu}_{12.5}\text{Be}_{22.5}$  bulk amorphous alloy. *Scr. Mater.* **54**, 483–487 (2006).
20. Wang, G. Y., Liaw, P. K., Yokoyama, Y. & Inoue, A. Size effects on the fatigue behavior of bulk metallic glasses. *J. Appl. Phys.* **110**, 113507 (2011).
21. Wang, G. Y., Liaw, P. K. & Morrison, M. L. Progress in studying the fatigue behavior of Zr-based bulk-metallic glasses and their composites. *Intermetallics* **17**, 579–590 (2009).
22. Yuan, T. *et al.* Modeling size effects on fatigue life of a zirconium-based bulk metallic glass under bending. *Acta Mater.* **61**, 273–279 (2013).
23. Jang, D., Gross, C. T. & Greer, J. R. Effects of size on the strength and deformation mechanism in Zr-based metallic glasses. *International Journal of Plasticity* **27**, 858–867 (2011).
24. Guo, H. *et al.* Tensile ductility and necking of metallic glass. *Nature Materials* **6**, 735–739 (2007).
25. Kumar, G., Desai, A. & Schroers, J. Bulk metallic glass: the smaller the better. *Advanced Materials* **23**, 461–476 (2011).
26. Tian, L. *et al.* Approaching the ideal elastic limit of metallic glasses. *Nature Communications* **3**, (2012).
27. Hammersley, A. P., Svensson, S. O., Hanfland, M., Fitch, A. N. & Hausermann, D. Two-dimensional detector software: From real detector to idealised image or two-theta scan. *High Pressure Res.* **14**, 235–248 (1996).
28. Wagner, C. N. J. Direct methods for the determination of atomic-scale structure of amorphous solids (x-ray, electron, and neutron-scattering). *Journal of Non-Crystalline Solids* **31**, 1–40 (1978).
29. Dmowski, W. *et al.* Structural rejuvenation in a bulk metallic glass induced by severe plastic deformation. *Acta Mater.* **58**, 429–438 (2010).
30. Jiang, W. H., Fan, G. J., Choo, H. & Liaw, P. K. Ductility of a Zr-based bulk-metallic glass with different specimen's geometries. *Materials Letters* **60**, 3537–3540 (2006).
31. Freels, M., Wang, G. Y., Zhang, W., Liaw, P. K. & Inoue, A. Cyclic compression behavior of a Cu-Zr-Al-Ag bulk metallic glass. *Intermetallics* **19**, 1174–1183 (2011).
32. Wang, G. Y., Demetriou, M. D., Schramm, J. P., Liaw, P. K. & Johnson, W. L. Compression-compression fatigue of  $\text{Pd}_{43}\text{Ni}_{10}\text{Cu}_{27}\text{P}_{20}$  metallic glass foam. *J. Appl. Phys.* **108**, 023505 (2010).
33. Weibull, W. A statistical distribution function of wide applicability. *Journal of Applied Mechanics-Transactions of the Asme* **18**, 293–297 (1951).



34. Wisnom, M. R. Size effects in the testing of fibre-composite materials. *Composites Science and Technology* **59**, 1937–1957 (1999).
35. Bigley, R. F. *et al.* Volume effects on fatigue life of equine cortical bone. *Journal of Biomechanics* **40**, 3548–3554 (2007).
36. Dempster, A. P., Laird, N. M. & Rubin, D. B. Maximum likelihood from incomplete data via em algorithm. *Journal of the Royal Statistical Society Series B-Methodological* **39**, 1–38 (1977).
37. Shi, Y. F., Louca, D., Wang, G. Y. & Liaw, P. K. Compression-compression fatigue study on model metallic glass nanowires by molecular dynamics simulations. *J. Appl. Phys.* **110**, 023523 (2011).
38. Jang, D., Maaß, R., Wang, G., Liaw, P. K. & Greer, J. R. Fatigue deformation of micro-sized metallic glasses. *Scr. Mater.* **68**, 773–776 (2013).
39. Schroeder, V., Gilbert, C. J. & Ritchie, R. O. A comparison of the mechanisms of fatigue-crack propagation behavior in a Zr-based bulk amorphous metal in air and an aqueous chloride solution. *Materials Science and Engineering a-Structural Materials Properties Microstructure and Processing* **317**, 145–152 (2001).
40. Schroeder, V., Gilbert, C. J. & Ritchie, R. O. Effect of aqueous environment on fatigue-crack propagation behavior in a Zr-based bulk amorphous metal. *Scr. Mater.* **40**, 1057–1061 (1999).
41. Gilbert, C. J., Ritchie, R. O. & Johnson, W. L. Fracture toughness and fatigue-crack propagation in a Zr-Ti-Ni-Cu-Be bulk metallic glass. *Applied Physics Letters* **71**, 476–478 (1997).
42. Kruzic, J. J. Predicting Fatigue Failures. *Science* **325**, (2009).

## Acknowledgements

The authors would like to acknowledge the financial support from the National Science Foundation (NSF), DMR-0909037, CMMI-0900271, and CMMI-1100080 with Drs. C.V. Cooper, A. Ardell, and E. Taleff as program directors. The authors are grateful to beamline scientists and staffs at the 1-ID and 11-ID stations of the Advanced Photon Source for their assistance in performing high-energy X-ray diffraction (XRD) experiments. W.D. would like to acknowledge the support from NSF, DMR-0906744.

## Author contributions

C.P.C. designed the experiment. C.P.C., G.Y. and M.F. performed the fatigue tests. C.P.C. and W.D. conducted the X.R.D. experiment and P.D.F. analysis. Y.T. did the statistical analysis and wrote the section. R.L. and Z.T. fabricated the materials used in the present study. C.P.C. analyzed the data and wrote the main manuscript. P.K.L. oversaw the project and provided guidance. All of co-authors reviewed the manuscript.

## Additional information

**Supplementary information** accompanies this paper at <http://www.nature.com/scientificreports>

**Competing financial interests:** The authors declare no competing financial interests.

**How to cite this article:** Chuang, C.-P. *et al.* Fatigue-Induced Damage in Zr-Based Bulk Metallic Glasses. *Sci. Rep.* **3**, 2578; DOI:10.1038/srep02578 (2013).



This work is licensed under a Creative Commons Attribution-NonCommercial-NoDerivs 3.0 Unported license. To view a copy of this license, visit <http://creativecommons.org/licenses/by-nc-nd/3.0>